Science of the Total Environment 890 (2023) 164084

Contents lists available at ScienceDirect

Science of the Total Environment

journal homepage: www.elsevier.com/locate/scitotenv

Struvite precipitation in wastewater treatment plants anaerobic digestion supernatants using a magnesium oxide by-product

V.B. Aguilar-Pozo [a,b], J.M. Chimenos [b], B. Elduayen-Echave [c,d], K. Olaciregui-Arizmendi [c,d], A. López [e], J. Gómez [e], M. Guembe [f], I. García [f], E. Ayesa [c,d], S. Astals [a,*]

[a] Department of Chemical Engineering and Analytical Chemistry, University of Barcelona, 08028 Barcelona, Spain
[b] Department of Materials Science and Physical Chemistry, University of Barcelona, 08028 Barcelona, Spain
[c] CEIT-Basque Research and Technology Alliance (BRTA), 20018 Donostia / San Sebastián, Spain
[d] Universidad de Navarra, Tecnun, 20018 Donostia / San Sebastián, Spain
[e] Navarra de Infraestructuras Locales S.A., 31008 Pamplona, Spain
[f] Magnesitas Navarras, S.A., 31630 Zubiri, Spain

HIGHLIGHTS

- LG-MgO by-product is an efficient reagent for struvite precipitation.
- The addition of LG-MgO released both magnesium and hydroxide ions.
- The P:Mg molar ratio controls the mineral phases of the precipitate.
- P:Mg molar ratios of 1:1 and 1:2 favour struvite precipitation.

GRAPHICAL ABSTRACT

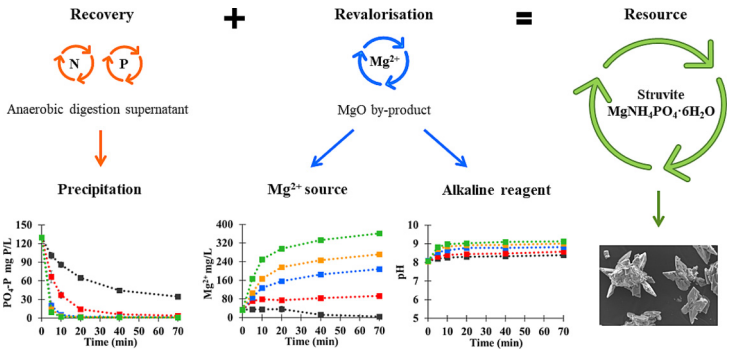

ARTICLE INFO

Editor: Huu Hao Ngo

Keywords:
Phosphorus recovery
Wastewater treatment
Magnesium ammonium phosphate
Magnesium by-product
Low-grade MgO
Circular economy

ABSTRACT

Struvite precipitation is a well-known technology to recover and upcycle phosphorus from municipal wastewater as a slow-release fertiliser. However, the economic and environmental costs of struvite precipitation are constrained by using technical-grade reagents as a magnesium source. This research evaluates the feasibility of using a low-grade magnesium oxide (LG-MgO) by-product from the calcination of magnesite as a magnesium source to precipitate struvite from anaerobic digestion supernatants in wastewater treatment plants. Three distinct LG-MgOs were used in this research to capture the inherent variability of this by-product. The MgO content of the LG-MgOs varied from 42 % to 56 %, which governed the reactivity of the by-product. Experimental results showed that dosing LG-MgO at P:Mg molar ratio close to stoichiometry (i.e. 1:1 and 1:2) favoured struvite precipitation, whereas higher molar ratios (i.e. 1:4, 1:6 and 1:8) favoured calcium phosphate precipitation due to the higher calcium concentration and pH. At a P:Mg molar ratio of 1:1 and 1:2, the percentage of phosphate precipitated was 53–72 % and 89–97 %, respectively, depending on the LG-MgO reactivity. A final experiment was performed to examine the composition and morphology of the precipitate obtained under the most favourable conditions, which showed that (i) struvite was the mineral phase with the highest peaks intensity and (ii) struvite was present in two different shapes: hopper and polyhedral. Overall,

Abbreviation: ANC, Acid neutralisation capacity; Ca^{2+}, Calcium ion; $CaCO_3$, Calcite; $CaMg(CO_3)_2$, Dolomite; $Ca_5(PO_4)_3(OH)$, Hydroxyapatite; EDS, Energy dispersive X-ray spectroscopy; EU, European Union; LG-MgO, Low-grade magnesium oxide; Mg^{2+}, Magnesium ion; $MgCO_3$, Magnesite; MgO, Magnesium oxide - periclase; $MgNH_4PO_4{\cdot}6H_2O$, Struvite; N, Nitrogen; P, Phosphorus; SEM, Scanning electron microscopy; TAN, Total ammoniacal nitrogen; TGA, Thermogravimetric analysis; WWTPs, Wastewater treatment plants; XRD, X-ray diffraction; XRF, X-ray fluorescence.

* Corresponding author.
E-mail address: sastals@ub.edu (S. Astals).

http://dx.doi.org/10.1016/j.scitotenv.2023.164084
Received 10 March 2023; Received in revised form 11 April 2023; Accepted 7 May 2023
Available online 18 May 2023

this research has demonstrated that LG-MgO is an efficient source of magnesium for struvite precipitation, which fits the circular economy principles by valorising an industrial by-product, reducing the pressure on natural resources, and developing a more sustainable technology for phosphorus recovery.

1. Introduction

Phosphorus is an essential, irreplaceable, and limited resource for human life. The European Union (EU) considers phosphorus one of the most critical raw materials due to its high economic importance, volatile price, and supply risk (Santos et al., 2021). EU countries are highly dependent on phosphate rock imports from Morocco, the United States and Kazakhstan (Kok et al., 2018). This dependency together with phosphorus losses throughout its life cycle requires technologies and policies that enforce phosphorus efficient management, recovery, and upcycling. The development of technologies for phosphorus recovery and upcycling from municipal wastewater is paramount since the largest phosphorus losses in the EU are from municipal sewage at around 1.2 g P/person/day (Muys et al., 2021; van Dijk et al., 2016).

Wastewater treatment plants (WWTPs) remove phosphorus from wastewater before it is discharged to prevent water bodies' eutrophication. In WWTP, phosphorus is typically removed by adding iron (e.g. $FeSO_4$, $FeCl_3$) or aluminium (e.g. $Al_2(SO_4)_3$, $AlCl_3$) salts to the activated sludge to precipitate insoluble phosphate salts (Kataki et al., 2016). These precipitates cannot be recovered since they are disposed of with the thickened biological sludge (de-Bashan and Bashan, 2004). However, Muys et al. (2021) estimated that phosphorus recovery in WWTPs through struvite ($MgNH_4PO_4{\cdot}6H_2O$) precipitation could satisfy about 13 % of the P-fertiliser demand in the EU.

Struvite is a valuable slow-release fertiliser with a reported market price ranging from 0 to 1000 €/t (Akyol et al., 2020; Muys et al., 2021). Struvite precipitation is a mature and efficient technology for phosphorus recovery in WWTPs. The precipitation reactor can be located in the anaerobic digestion centrate sidestream that recirculates the anaerobic digestion dewatering liquor back to the mainline water treatment process, due to its relatively high phosphate and ammonium concentration, low organic matter content, and small flow rate (<0.3 % of the WWTP inflow) (Martí et al., 2010; Uysal et al., 2010). However, struvite precipitation in WWTP requires the addition of a Mg^{2+} source since struvite precipitation occurs with a Mg:N:P molar ratio of 1:1:1 when the concentrations of precursors exceed the struvite solubility product constant (Kazadi Mbamba et al., 2015; Siciliano et al., 2020).

$MgCl_2{\cdot}6H_2O$ and $Mg(OH)_2$ are the most common magnesium sources in full-scale applications (Muys et al., 2021; Rahman et al., 2014). $MgCl_2{\cdot}6H_2O$ and $Mg(OH)_2$ are dosed at P:Mg ratio between 1.2 and 2.0 (Crutchik et al., 2017; Muys et al., 2021). The optimum pH range for struvite precipitation is 8.0–9.5 (Battistoni et al., 2001; Doyle and Parsons, 2002; Rahman et al., 2014). The use of $MgCl_2{\cdot}6H_2O$ or $Mg(OH)_2$ typically requires the dosage of an alkali (typically NaOH) or energy for CO_2 stripping to increase and control the pH in the reactor (Muys et al., 2021; Siciliano et al., 2020).

Reagent consumption is the main cost contributor to struvite precipitation (Vinardell, 2021). $MgCl_2{\cdot}6H_2O$ has a cost of around 370 €/t (~3100 €/t_{Mg}), $Mg(OH)_2$ around 350 €/t (~840 €/t_{Mg}) and NaOH around 620 €/t (Bouzas et al., 2019; Crutchik et al., 2017). Using technical-grade reagents also results in significant environmental impacts, limiting the environmental benefits of struvite precipitation in WWTP (Amann et al., 2018; Bradford-Hartke et al., 2015; Sena et al., 2021). Sena et al. (2021) advocated the search for an alternative source of magnesium and pH control to make the struvite precipitation process environmentally friendly and economically viable.

Researched magnesium alternative sources include seawater and brine (Bradford-Hartke et al., 2021), wood ash (Park et al., 2021), bittern (El Diwani et al., 2007), and MgO by-products (Chimenos et al., 2003; Quintana et al., 2004; Romero-Güiza et al., 2015). MgO by-products from the calcination of magnesite (a.k.a. low-grade MgO (LG-MgO)) are a potential source of magnesium for struvite precipitation since (i) it is much cheaper than $MgCl_2{\cdot}6H_2O$ and $Mg(OH)_2$ (LG-MgO price: ~100 €/t, ~220 €/t_{Mg}), (ii) hydration and dissolution of MgO releases hydroxyls ions which increases pH, reducing the need of dosing NaOH or stripping CO_2, (iii) some technologies already use high-grade MgO as magnesium source (e.g. Anphos, Phospaq), which eases the adoption of this by-product as an alternative reagent, (iv) it has a relatively low heavy metals content, and (v) it fits the circular economy principles by valorising and industrial by-product, reducing the pressure on natural resources, and developing more sustainable technology for phosphorous recovery.

Chimenos et al. (2003), Quintana et al. (2004, 2005, 2008) and Romero-Güiza et al. (2015) successfully used LG-MgO to precipitate struvite from different waste streams. Chimenos et al. (2003) observed struvite precipitation onto the LG-MgO particles, a struvite coating layer that could have limited MgO dissolution and efficiency. Quintana et al. (2005, 2008) reported that smaller LG-MgO particles displayed higher phosphate removal efficiencies than raw and milled LG-MgO particles, likely due to a larger reactive area. Quintana et al. (2005, 2008) and Romero-Güiza et al. (2015) reported that high-grade MgO particles yielded better phosphorus removal efficiencies than LG-MgO, probably due to its higher reactivity. However, Romero-Güiza et al. (2015) noted that the reagent efficiency to precipitate struvite was only partly dictated by the MgOs reactivity. The reactivity of LG-MgO by-product depends on several factors, mainly composition of the raw material, calcination temperature, calcination time, and particle size (del Valle-Zermeño et al., 2016; del Valle-Zermeño et al., 2015). Therefore, the utilisation of LG-MgO by-products as a magnesium source for struvite precipitation requires understanding which are the mechanisms that govern the LG-MgO reagent efficiency and how these relate to LG-MgO properties. This knowledge is important to tune the precipitation process (e.g. contact time and dosing strategy) based on LG-MgO properties.

The goal of this study was to evaluate the feasibility of using a LG-MgO by-product as a magnesium source to precipitate struvite from WWTP anaerobic digestion supernatants. To reach this goal, three different LG-MgO were characterised and used for struvite precipitation under different P:Mg molar ratios. A final experimental trial was carried out to analyse the composition and morphology of the precipitate obtained under the most favourable conditions.

2. Materials and methods

2.1. Wastewater and magnesium by-products origin

The anaerobic digestion supernatant used in this research was collected from a mesophilic anaerobic digester of a municipal WWTP in Navarra (Spain). At the WWTP, the supernatant is obtained by centrifuging the effluent of the anaerobic digester (Fig. 1). After shipment, the supernatant was stored in a fridge at 4 °C to minimise its degradation (maximum storage time of 3 weeks). Before each experiment, the pH and concentrations of phosphorus, magnesium, calcium, and ammoniacal nitrogen were measured to ensure that the properties of the supernatant remained constant.

The LG-MgO by-products used as a magnesium source for struvite precipitation were provided by Magnesitas Navarras, S.A. (Navarra, Spain). Specifically, LG-MgO by-products were collected from the fabric filters arranged in the exhaust gas pollution control system that drags fine particles of the rotatory kiln calcinating natural magnesite to produce commercial MgO products. Three LG-MgO by-products were used in this study

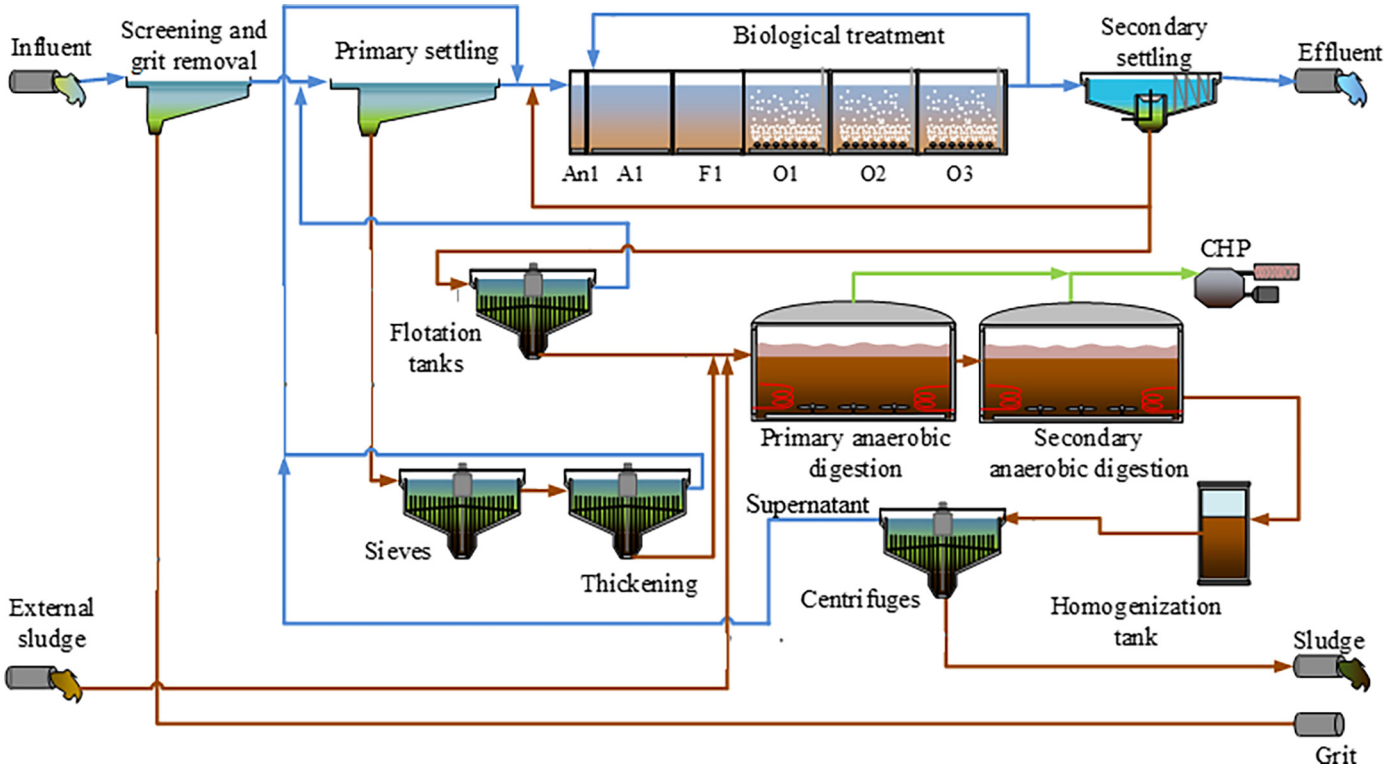

Fig. 1. Process flow diagram of the municipal WWTP in Navarra (Spain).

(named hereafter LG-MgO_A, LG-MgO_B, and LG-MgO_C) to assess the impact of their inherent variability on struvite precipitation.

2.2. Analytical methods

pH and conductivity were measured using a MultiMeter MM41 (Crison) equipped with a pH electrode (Crison, 50 52) and a conductivity electrode (Crison, Pt 1000). Total alkalinity was measured following the Standard Method 2320B with an automatic titrator instrument (Crison, pH-Burette 24) dosing 0.1 M HCl and a pH endpoint of 4.30. Cations (Ca^{2+}, Mg^{2+}) and anion (PO_4-P) were analysed using an 861 Advanced Compact IC Metrohm ionic chromatographer equipped with Metrosep columns (Metrosep C 4–150/4.0 and Metrosep A Supp 17–250/4.0, respectively) and following the manufacturer's protocol. Total ammoniacal nitrogen (TAN) was also analysed by ionic chromatography. Before ions analysis, the samples were filtered through a 0.45 μm regenerated cellulose syringe filter.

The composition of the solid samples was determined by X-ray fluorescence (XRF), X-ray diffraction (XRD), thermogravimetric analysis (TGA) and scanning electron microscopy (SEM) combined with energy dispersive X-ray spectroscopy (EDS). The major and minor elemental composition, expressed as the most stable oxides at 1050 °C, was determined by XRF using a Philips PW2400 X-ray sequential spectrophotometer. Crystalline mineral phases were identified by XRD using a Bragg–Brentano Siemens D-500 powder diffractometer device using CuK_α radiation. The X'Pert HighScore program was used to determine the mineral phases. SEM micrographs were obtained with a Quanta 200 FEI scanning electron microscope. EDS analysis was used to obtain information about the microscale (around 1 μm^3) elemental composition and chart compositional changes along the sample surface. The weight loss percentage of the volatile compound of each mineral phase was identified by TGA using a SDT Q600 Simultaneous TGA-DSC (TA Instruments, US) under a N_2 inert gas atmosphere. In the TGA analysis, the temperature increased from 30 to 1400 °C at a heating rate of 10 °C/min. The particle size distribution was determined by a LS 13320 Beckman Coulter laser diffraction particle size analyser. The specific surface area was determined with the BET single-point method using a Micrometrics Tristar 3000 porosimeter. The LG-MgO reactivity was determined using the citric acid reactivity test, which measures the time required by 2.0 g of sample in 100 mL of 0.4 N citric acid solution to reach pH 8.6 (del Valle-Zermeño et al., 2016). The reactivity of MgOs can be classified into four categories depending on the time need to reach pH 8.6, i.e. highly reactive (<60 s), medium reactive (180–300 s), low reactive (>600 s) and barely reactive (>900 s) (Strydom, 2005). The acid neutralisation capacity (ANC) was carried out to determine the buffer capacity of the LG-MgOs. Briefly, 3 g of LG-MgO were added to 300 mL of deionised water and stirred for 1 hour. Then, nitric acid (5 M) was gradually added until the solution reached pH 4 (del Valle-Zermeño et al., 2016).

2.3. Experimental set-up

2.3.1. Dissolution capacity of LG-MgO in deionised water

The dissolution capacity of the three LG-MgO in deionised water aimed to evaluate the solubility of the LG-MgO particles without interference from other ions. Experiments were carried out in a jar test device (Velp Scientifica® JT6) with a beaker containing 0.5 L of deionised water, under continuous mixing (200 rpm) and at room temperature (ca. 20 °C). Five different LG-MgO concentrations were tested for each LG-MgO sample. The tested LG-MgO concentrations were those that led to a P:Mg molar ratio of 1:1, 1:2, 1:4, 1:6 and 1:8 when considering the supernatant phosphate concentration of 132 mg P/L. The LG-MgOs magnesium concentration was calculated from the composition of each by-product. During the experiments, pH, anions and cations were measured at 0, 30, 60, 120, and 180 min. All experiments were carried out by duplicate.

2.3.2. Effect of increasing the pH of the supernatant

This experimental trial was carried out to assess if increasing the supernatant pH from 7.9 to 8.5, 9.0 or 9.5 (4 M NaOH) was sufficient to partially or completely precipitate the phosphate present in the supernatant. Once the targeted pH was reached, pH and anions and cations were measured at 0, 5, 10, 20, and 40 min. These experiments were carried out in a beaker

Table 1
Properties and mineral composition of the three LG-MgOs.

	Units	LG-MgO_A	LG-MgO_B	LG-MgO_C
Mineral composition				
Al_2O_3	%	0.29	0.38	0.36
$CaCO_3$	%	11.59	10.37	11.58
$CaMg(CO_3)_2$	%	8.55	5.67	6.29
$Ca(OH)_2$	%	2.24	1.00	0.00
$CaSO_4$	%	1.71	3.20	2.87
Fe_2O_3	%	2.31	2.16	2.20
$MgCO_3$	%	12.04	21.71	25.99
MgO	%	56.04	47.80	42.46
$Mg(OH)_2$	%	3.75	2.89	3.52
$MgSO_4$	%	–	3.11	1.94
SiO_2	%	1.49	2.13	2.14
Properties				
Reactivity	s	150	680	1608
Specific surface area	m^2/g	14.64	12.80	11.90
Mean diameter	μm	12.20	22.70	25.90
Porosity	–	0.57	0.54	0.55

containing 0.5 L of the anaerobic digestion supernatant at room temperature (ca. 20 °C) in a jar test device under continuous mixing (200 rpm). All pH conditions were carried out by duplicate.

2.3.3. Struvite precipitation with LG-MgO at different P:Mg molar ratio

Struvite precipitation experiments were carried out at five different P:Mg molar ratios (i.e. 1:1, 1:2, 1:4, 1:6, and 1:8) for each of the three LG-MgO. These experiments aimed to find the most suitable P:Mg molar ratio as well as to assess the response of each LG-MgO under similar experimental conditions. It is worth noting that the pH of the supernatant was not adjusted, thus, pH changes were related to the basicity provided by the LG-MgO and those caused by precipitation of struvite and/or other minerals. During the experiments, pH, anions, and cations were measured at 0, 5, 10, 20, 40, and 70 min. The experiments were carried out in a beaker containing 0.5 L of anaerobic digestion supernatant at room temperature (ca. 20 °C) in a jar test device under continuous mixing (200 rpm). All conditions were carried out by duplicate.

2.3.4. Analysis of the precipitate composition

A final experiment was carried out to analyse the composition of the precipitate obtained using the most favourable struvite precipitation conditions from Section 2.3.3 (i.e. LG-MgO_A, P:Mg molar ratio of 1:2 and without pH adjustment). The experiment was carried out in an 8 L glass reactor equipped with an anchor agitator. Specifically, 7 L of anaerobic digestion supernatant at room temperature (ca. 20 °C) reacted with 3.64 g LG-MgO_A for 70 min under continuous mixing (250 rpm). The pH, anions and cations were measured at the beginning and the end of the experiment. After 70 min, the mixing was stopped to facilitate the sedimentation of the particles from the supernatant. The filtered particles were dried at 30 °C (to prevent loss of struvite hydration water) in a temperature controlled-incubator for 48 h. The dry particles were characterised by XRD and SEM-EDS.

2.4. Calculations

The mineral composition of the three LG-MgO by-products was estimated by combining the XRF, XRD and TGA results. Briefly, the mineral phases of the solid were identified by XRD and quantified by TGA, except for the oxides. The TGA diffractogram provides the weight loss percentage of the volatile compound of each mineral phase through its decomposition temperature range. The percentage of the mineral phases in the solid was calculated by combining the percentage of weight loss and its decomposition reaction (e.g. $MgCO_{3(s)} \rightarrow MgO_{(s)} + CO_{2(g)}$ at 450–625 °C). Finally,

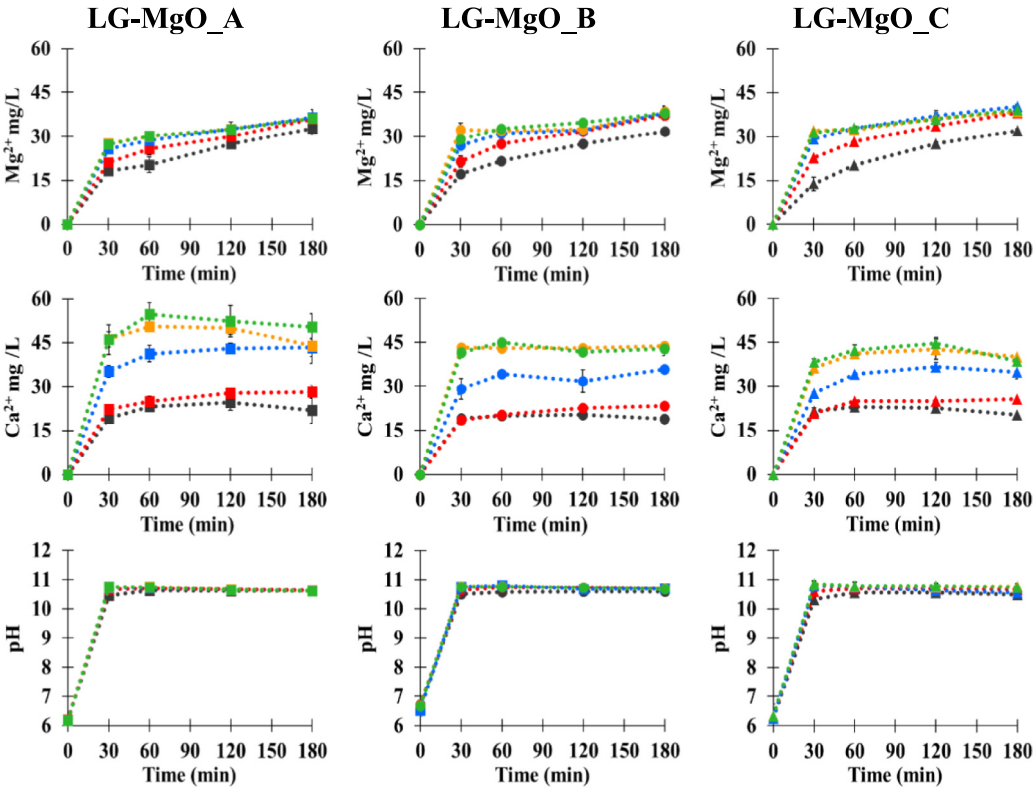

Fig. 2. Dissolution of (left) LG-MgO_A, (center) LG-MgO_B, and (right) LG-MgO_C in deionised water. (top) Mg^{2+} concentration, (middle) Ca^{2+} concentration and (bottom) pH. P:Mg molar ratio of (■) 1:1, (■) 1:2, (■) 1:4, (■) 1:6, (■) 1:8. Error bars show the standard deviation among replicates.

the percentage of oxide in the sample was calculated as the difference between the total oxide percentage obtained by XRF and the oxide percentage calculated from the non-oxide mineral phases identified by XRD and TGA.

3. Results and discussion

3.1. Characterisation of the LG-MgO by-products

Table 1 shows the properties and mineral composition of the three LG-MgO by-products. Periclase (MgO) was the main mineral phase in the LG-MgOs followed by magnesite ($MgCO_3$) and calcite ($CaCO_3$). LG-MgO_A had the highest content of MgO (56 %) followed by LG-MgO_B (48 %) and LG-MgO_C (42 %). The presence of $MgCO_3$, $CaCO_3$, and $CaMg(CO_3)_2$ in the LG-MgOs is related to unreacted material due to the short residence time of the particles in the rotatory kiln during the calcination of natural magnesite. The presence of sulphates is attributed to the reaction of basic compounds with sulphur dioxide (SO_2) from fossil fuel flue gases. All the LG-MgOs contained small amounts of Al_2O_3, Fe_2O_3, $Mg(OH)_2$, $MgSO_4$ and SiO_2, among others. The different composition of the LG-MgO could be due to the initial composition of the raw material, contact time and calcination temperature (del Valle-Zermeño et al., 2015).

LG-MgO_A showed the highest citric acid reactivity (150 s) followed by LG-MgO_B (680 s) and LG-MgO_C (1608 s). According to Strydom (2005), LG-MgO_A classifies as medium reactive, LG-MgO_B as low reactive and LG-MgO_C as barely reactive. The higher reactivity of the LG-MgO_A can be attributed to its higher percentage of MgO, $Mg(OH)_2$ and $Ca(OH)_2$ (Romero-Güiza et al., 2015) as well as its higher specific surface area. The mean diameter of the LG-MgO_A particles was 12 μm, about half the diameter of LG-MgO_B (23 μm) and LG-MgO_C (26 μm). A smaller particle size (higher specific surface area) implies that more particle surface was in contact with the calcination temperature in the rotatory kiln, which could explain the higher content of MgO in LG-MgO_A. The porosity of the three LG-MgOs was similar with values ranging between 0.54 and 0.57 (Table 1).

3.2. Characterisation of the mesophilic anaerobic digestion supernatant

The phosphate, TAN and magnesium concentrations in the anaerobic digestion supernatant were 132 mg P/L, 1356 mg N/L and 36 mg Mg^{2+}/L, respectively. The phosphate concentration was higher than 50 mg P/L, which has been reported as the threshold concentration for the economic viability of struvite precipitation (Desmidt et al., 2013). The P:Mg molar ratio in the supernatant was 1:0.35, which is lower than the minimum required 1:1 stoichiometric ratio. Therefore, a magnesium source is needed to favour struvite precipitation. The supernatant had an excess of TAN, which shifts the reaction towards the formation of struvite based on Le Chatelier's principle (Eq. (1)). The calcium concentration of the supernatant was 160 mg Ca^{2+}/L. It has been reported that high calcium concentrations interfere with struvite precipitation since calcium can precipitate with phosphate, decreasing its availability. In addition, calcium ions interfere with the shape, size, induction time and purity of the struvite (Bayuseno and Schmahl, 2020; Liu and Wang, 2019; Pastor et al., 2008). The supernatant had a pH of 7.98, a total alkalinity of 4465 mg $CaCO_3$/L, and a conductivity of 10.52 mS/cm.

The chemical reaction of struvite formation is depicted in Eq. (1), where n can be 0, 1 or 2 depending on the pH of the solution (Ariyanto, 2014). Given that the pH values in the supernatant and the precipitation experiments were between 8.0 and 9.2, the phosphate species in equilibrium were mainly $H_2PO_4^-$ and HPO_4^{2-}.

$$Mg^{2+} + NH_4^+ + H_nPO_4^{n-3} + 6H_2O \leftrightarrow MgNH_4PO_4 \cdot 6H_2O + nH^+ \quad (1)$$

3.3. LG-MgOs dissolution in deionised water

Fig. 2 illustrates the Mg^{2+} and Ca^{2+} released and the change in pH when the three LG-MgO by-products were dissolved in deionised water at five different doses. Table 2 shows the Mg^{2+} and Ca^{2+} dissolution yield, i.e., grams of element released per gram of LG-MgO added.

The final Mg^{2+} concentration was very similar for the three LG-MgOs at 38 mg Mg^{2+}/L regardless of the P:Mg molar ratio, except for the 1:1 molar ratio, which had a final concentration of 32 mg Mg^{2+}/L. The release of Mg^{2+} occurred mainly during the first 30 min and slowed down once the solution pH reached 10.7. The rapid pH increase can be explained by the hydroxylation of MgO into $Mg(OH)_2$, and the subsequent release of Mg^{2+}, and OH^- into the solution. According to the MgO hydration mechanism proposed by Stolzenburg et al. (2015), the release of Mg^{2+} and OH^- stops once their concentrations reach the supersaturation, where $Mg(OH)_2$ precipitates and covers the particle preventing further MgO hydroxylation. Considering the solubility product constant of $Mg(OH)_2$ ($K_{sp} = 3.4{\cdot}10^{-11}$), the pH of $Mg(OH)_2$ dissolution at equilibrium is around 10.5 (Amaral et al., 2007). Table 2 shows that the Mg^{2+} released per gram of LG-MgO into the solution was inversely proportional to the amount of LG-MgO added. These results illustrate that the dissolution of Mg^{2+} from LG-MgO in deionised water is limited by chemical equilibrium, i.e., magnesium was released until the activity product between Mg^{2+} and OH^- reached the K_{sp}. Thus, adding more LG-MgO did not result in higher Mg^{2+} concentrations.

Unlike Mg^{2+}, the final Ca^{2+} concentration increased as the P:Mg molar ratio increased from 1:1 to 1:8 (Fig. 2). The release of Ca^{2+} occurred mainly during the first 60 min followed by a slight drop in concentration. The final drop in Ca^{2+} concentration could be explained by the formation of $Ca(OH)_2$ on the LG-MgO surface due to a localised level of supersaturation at the particles boundary layer (Stolzenburg et al., 2015). The increase in Ca^{2+} concentration was inversely proportional to the amount of LG-MgO added (Table 2).

3.4. Effect of increasing the pH of the supernatant

Fig. 3 shows a small drop in phosphate concentrations when the supernatant pH was increased from 7.98 to 8.5, 9.0 and 9.5. Specifically, the phosphate concentration decreased from 125 mg P/L to 114, 113, and 108 mg P/L, respectively. Calcium also showed a minor drop in concentration, while the magnesium concentrations had slight fluctuation during the experiment (Fig. 3). At pH 9.0 and 9.5, the TAN concentration decreased from 1328 to 1260 mg N/L, probably due to ammonia stripping. TAN stripping at pH 8.5 was minimal, with a final TAN concentration of 1313 mg N/L.

The slight reduction in phosphate concentration was related to the precipitation of calcium phosphate salts, which is favoured at pH 8–10 (Ye et al., 2017). However, these results indicate that (i) simply increasing the pH would not lead to significant changes in phosphate concentration and

Table 2
Mg^{2+} and Ca^{2+} dissolution yield in deionised water (gram of ions released LG-MgO added). Results are expressed as average ± standard deviation.

	1:1	1:2	1:4	1:6	1:8
g Mg^{2+}/g LG-MgO_A	0.126 ± 0.007	0.069 ± 0.006	0.034 ± 0.001	0.023 ± 0.001	0.017 ± 0.001
g Mg^{2+}/g LG-MgO_B	0.109 ± 0.003	0.064 ± 0.002	0.033 ± 0.002	0.020 ± 0.001	0.015 ± 0.001
g Mg^{2+}/g LG-MgO_C	0.109 ± 0.003	0.064 ± 0.002	0.033 ± 0.002	0.020 ± 0.001	0.014 ± 0.001
g Ca^{2+}/g LG-MgO_A	0.084 ± 0.017	0.054 ± 0.004	0.042 ± 0.003	0.028 ± 0.004	0.024 ± 0.002
g Ca^{2+}/g LG-MgO_B	0.065 ± 0.005	0.040 ± 0.001	0.031 ± 0.001	0.022 ± 0.001	0.016 ± 0.001
g Ca^{2+}/g LG-MgO_C	0.065 ± 0.005	0.040 ± 0.001	0.031 ± 0.001	0.022 ± 0.001	0.016 ± 0.001

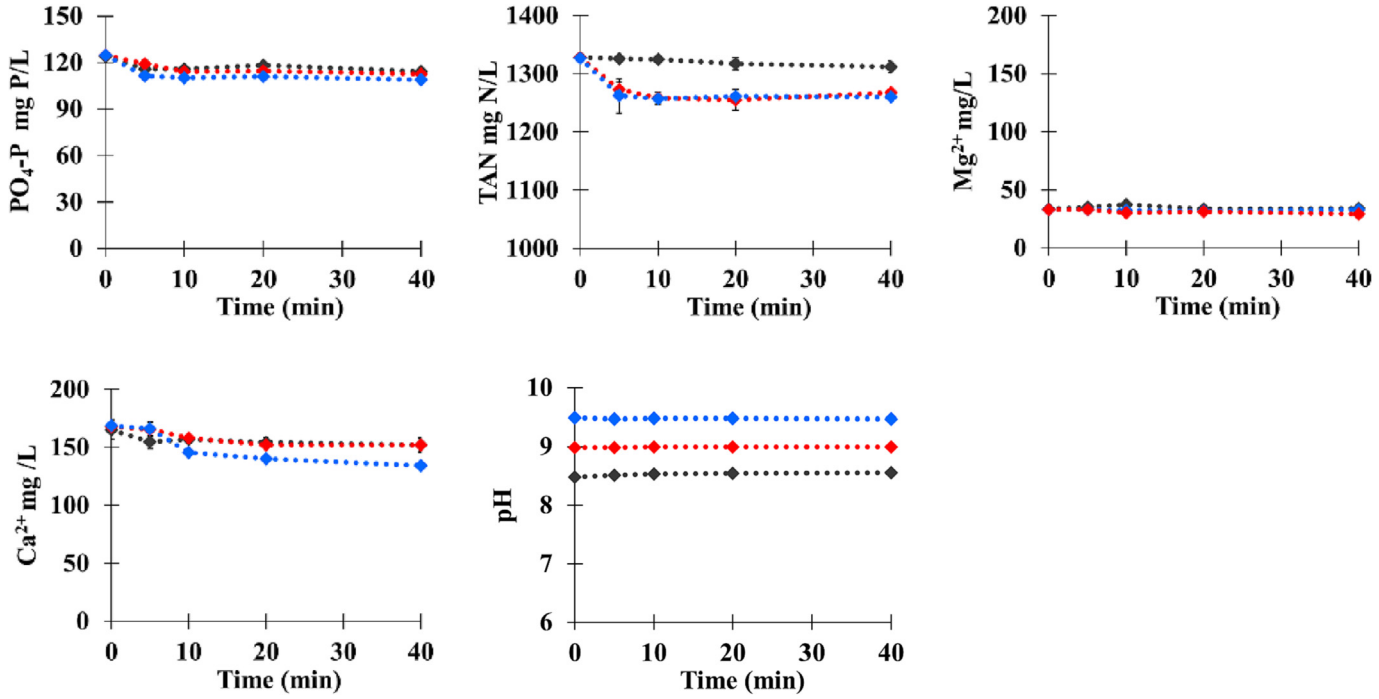

Fig. 3. Experimental results from increasing the anaerobic digestion supernatant pH to (●) 8.5, (●) 9.0 and (●) 9.5. Error bars show the standard deviation among replicates.

(ii) the supernatant did not have the composition required to precipitate all the phosphate. Accordingly, the addition of a magnesium source is needed to reach the supersaturated state required to favour struvite precipitation (Marti et al., 2008).

3.5. Struvite precipitation with LG-MgO at different P:Mg molar ratio

Dosing LG-MgOs decreased the phosphate concentration of the supernatant (Fig. 4). The rate of phosphate precipitation depended on the P:Mg molar ratio and, to a lesser extent, the LG-MgO sample (i.e. LG-MgO_A, LG-MgO_B, LG-MgO_C). In general, the higher the LG-MgO reactivity, the higher the Mg^{2+} dissolution and pH. The experiments carried out with a P:Mg molar ratio of 1:8 and 1:6 showed a similar capacity to precipitate phosphate since both decreased the phosphate concentration from 130 to <20 mg P/L in 5 min regardless of the LG-MgO sample (Fig. 4). The experiments carried out with a P:Mg molar ratio of 1:4 were slightly slower, but they were able to reach phosphate concentrations <20 mg/L in 10 min (Fig. 4). The difference in LG-MgOs reactivity was more evident when the P:Mg molar ratio decreased. At a P:Mg molar ratio of 1:2, LG-MgO_A was able to reach phosphate concentration <20 mg P/L in 20 min, while LG-MgO_B and LG-MgO_C reached that concentration after 70 min (Fig. 4). The calcium concentration was similar for the three LG-MgO samples at about 150 mg Ca^{2+}/L.

The experiments carried out using a P:Mg molar ratio of 1:2 and 1:1 reached a maximum pH of 8.5, limiting ammonium stripping. Fig. 4 shows an equimolar decrease in the phosphate and TAN concentrations over time, following the stoichiometry of the struvite reaction (Eq. (1)). This equimolar consumption indicated that struvite was the main precipitation product under these experimental conditions (see Table SI in the supplementary material). The phosphate precipitation efficiency ranged between 89 and 97 % and between 53 and 72 % for the experiments carried out at a P:Mg molar ratio of 1:2 and 1:1, respectively. It is worth noting that the change in Mg^{2+} concentration cannot be used to calculate the moles of Mg^{2+} precipitated since it comprises two phenomena: (i) Mg^{2+} ions released from LG-MgOs, and (ii) Mg^{2+} precipitated. However, the negative net change in Mg^{2+} concentration indicated that there was more precipitation than release.

The experiments carried out at a P:Mg molar ratio of 1:8, 1:6 and 1:4 showed a different trend, i.e. a net decrease in Ca^{2+} concentration over time (particularly in the first 10 min) (Fig. 4). These results showed that the Ca^{2+} from the supernatant and released from the LG-MgO particles precipitated with phosphate. These results indicated that a high LG-MgO dosing would favour the precipitation of calcium phosphate instead of struvite precipitation due to the higher Ca^{2+} concentration and pH. In these experiments, there was a net increase in Mg^{2+} concentration, indicating that more Mg^{2+} was released from the LG-MgO particles than precipitated as struvite. The final Mg^{2+} concentration increased as the LG-MgO reactivity increased. These results align with those reported by Hao et al. (2008), who observed that the struvite content of the precipitate decreased as the solution pH increased. Specifically, at pH 7.5 the struvite content was 96 % and at pH 10.5 it was 16 %, while no struvite was detected at pH values above 10.5. Finally, it is worth mentioning that the dissolution of LG-MgO in the supernatant was much higher than in deionised water (see Section 3.3). This behaviour could be attributed to the buffering capacity of the supernatant, which limited the pH increase and favoured LG-MgO dissolution.

3.6. Characterisation of the precipitate

Fig. 5 shows the XRD pattern and the identified mineral phases of the precipitate obtained in the experiment carried out in a 7 L reactor using LG-MgO_A, a P:Mg molar ratio of 1:2 ratio and no pH adjustment. Struvite was the mineral phase with the highest peak intensity followed by magnesite, magnesium oxide, dolomite, hydroxyapatite, and calcium carbonate. Struvite and hydroxyapatite were the new-formed mineral phases in the solid fraction since the other phases were already present in the LG-MgO (Table 1). These phases did not dissolve in the solution due to (i) its low K_{sp} value, (ii) a short contact time and/or (iii) coating of the LG-MgO particles by precipitation of new-formed mineral phases on the surface of the particles. The supernatant pH reached 8.46 and the decrease of TAN (from 1321 to 1263 mg N/L) and phosphate (from 133 to 3 mg P/L) concentration in the experiment was practically equimolar, reaffirming that these operational conditions favour struvite precipitation.

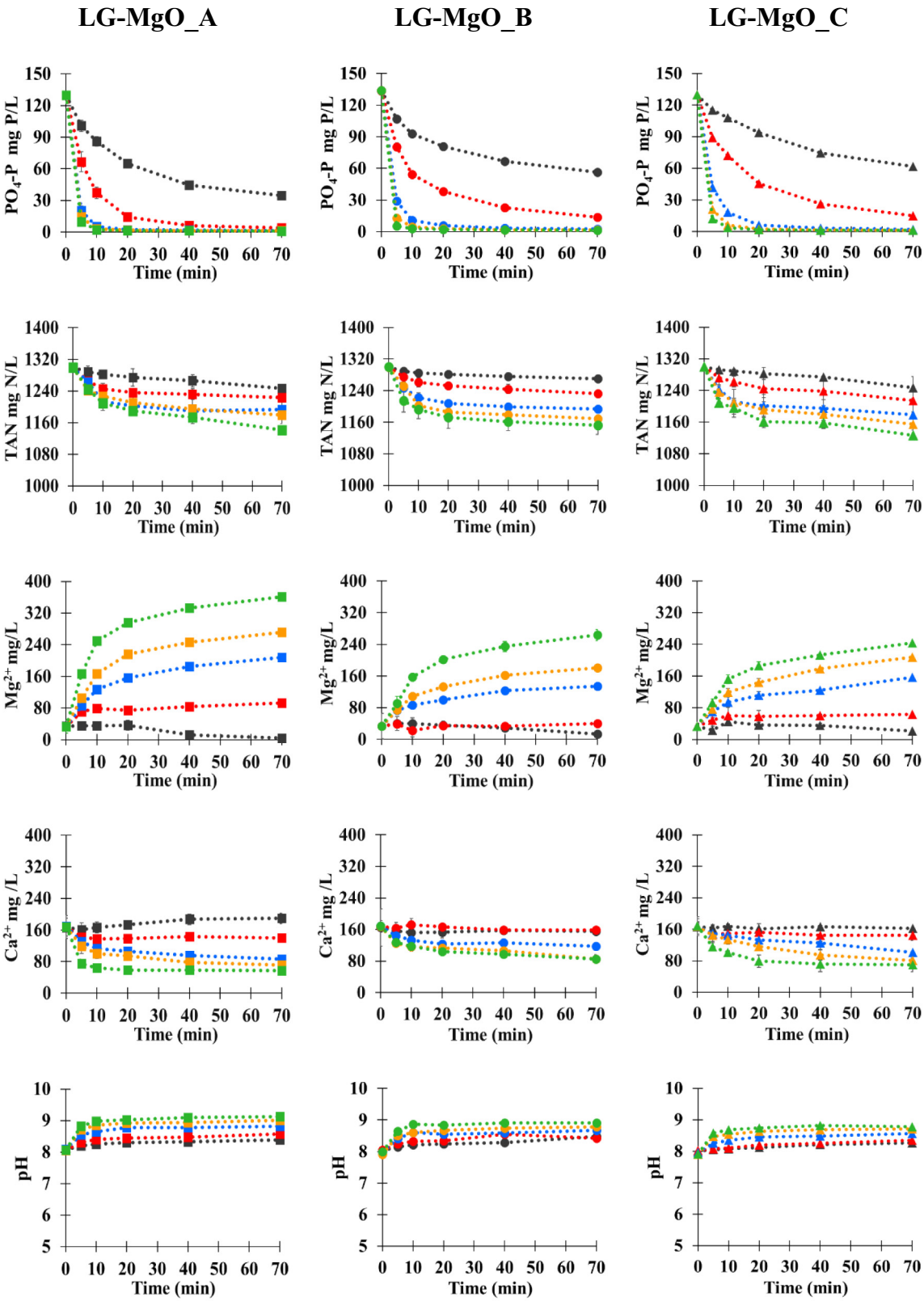

Fig. 4. Precipitation and dissolution of (left) LG-MgO_A, (centre) LG-MgO_B, and (right) LG-MgO_C in the anaerobic digestion supernatant. P:Mg molar ratio of (■) 1:1, (■) 1:2, (■) 1:4, (■) 1:6, (■) 1:8. Error bars show the standard deviation among replicates.

The SEM micrograph in Fig. 6 shows the morphology of the precipitate, where five main shapes could be distinguished: (1) hopper, (2) polyhedral, (3) partly-dissolved LG-MgO particle, (4) agglomeration of polyhedral on LG-MgO particles, and (5) agglomeration of polyhedral. Fig. 6 also shows the elemental composition of five spots (red crosses) analysed by EDS. The hopper (spot 1) and polyhedral (spot 2) are struvite crystals, which

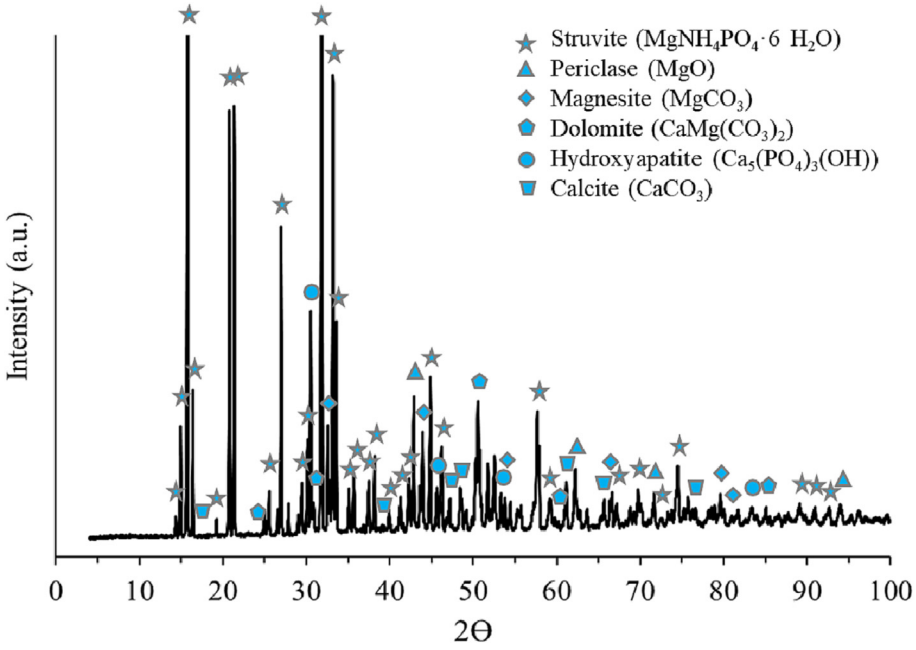

Fig. 5. Results from XRD analysis of the precipitate obtained using LG-MgO_A and a P:Mg molar ratio of 1:2 ratio.

formation has been related to differences in oversaturation and pH (Elduayen-Echave et al., 2020; Shaddel, 2019). Specifically, hopper particles have been reported to form at high pH and highly oversaturated solutions, while polyhedral particles formation are favoured at lower alkaline pH and less oversaturated solutions (Elduayen-Echave et al., 2020). In this experiment, the pH increased from 7.96 to 8.46 and the Mg^{2+} concentration from 34 to 78 mg/L. Therefore, the initial conditions (lower pH and Mg^{2+} concentrations) could have favoured the formation of polyhedral struvite crystals, while the final conditions could have favoured the formation of hopper struvite crystals formation (higher pH and Mg^{2+} concentrations).

The main mineral phase identified in the diffractogram was struvite (hopper and polyhedral particles), indicating that most of the MgO dissolves are available for struvite precipitation. In addition, two types of agglomeration were also observed, polyhedral agglomeration on LG-MgO particle surface (spot 4), and polyhedral agglomeration (spot 5). The agglomeration of particles is favoured at high pHs and Mg^{2+} concentrations since the zeta-potential decreases favouring particles agglomeration (Fromberg et al., 2020). The irregular shapes observed in the micrograph (spots 3 and 4) were identified as LG-MgO particles, although phosphorus was present on their surface. These results suggest the presence of other mineral phases in spot 3 and spot 4 such as hydroxyapatite, newberyite and bobierrite. Newberyite and bobierrite were not detected in the XRD analysis of the precipitate (Fig. 5), which could be due to their low content (<2 %).

4. Conclusions

LG-MgO by-products from the calcination of magnesite represent an effective source of magnesium to precipitate struvite from WWTP anaerobic digestion supernatants regardless of their composition. The amount of MgO in the LG-MgOs varied from 42 % to 56 %, where higher MgO percentages led to higher reactivities. Experimental results showed that dosing LG-MgO at P:Mg molar ratio close to stoichiometry (i.e. 1:1 and 1:2) favoured struvite precipitation, whereas higher P:Mg molar ratios (i.e. 1:4, 1:6 and 1:8) favoured calcium phosphate precipitation due to the higher calcium concentration and pH. At a P:Mg molar ratio of 1:1 and 1:2, the percentage of phosphate precipitated was 53–72 % and 89–97 %, respectively, depending on the LG-MgO sample reactivity. The precipitate obtained from an experiment carried out at a P:Mg molar ratio of 1:2 and no pH control showed that (i) struvite was the main mineral phase and (ii) struvite was present in two different shapes: hopper and polyhedral. The latter indicates that two distinct reaction mechanisms take place during the precipitation process.

Supplementary data to this article can be found online at https://doi.org/10.1016/j.scitotenv.2023.164084.

CRediT authorship contribution statement

V.B. Aguilar-Pozo: Investigation, Formal analysis, Validation, Writing – original draft. **J.M. Chimenos:** Conceptualization, Supervision, Writing – review & editing, Funding acquisition. **B. Elduayen-Echave:** Investigation, Funding acquisition, Writing - review & editing. **K. Olaciregui-Arizmendi:** Investigation, Validation. **A. López:** Resources, Validation. **J. Gómez:** Validation, Funding acquisition. **M. Guembe:** Resources, Validation. **I. García:** Resources, Funding acquisition. **E. Ayesa:** Conceptualization, Supervision, Writing – review & editing, Funding acquisition. **S. Astals:** Conceptualization, Methodology, Supervision, Writing – review & editing, Funding acquisition.

Data availability

Data will be made available on request.

Declaration of competing interest

The authors declare the following financial interests/personal relationships which may be considered as potential competing interests:

Andrea Lopez reports financial support was provided by Spain Ministry of Science and Innovation. Sergi Astals reports financial support was provided by Spain Ministry of Science and Innovation. Veronica Aguilar reports financial support was provided by Government of Catalonia Agency for Administration of University and Research Grants.

Acknowledgements

This research was supported by the grant RTC2019-007257-5 funded by the Spanish Ministry of Science and Innovation MCIN/AEI /10.13039/501100011033. Verónica B. Aguilar is grateful to the Generalitat de

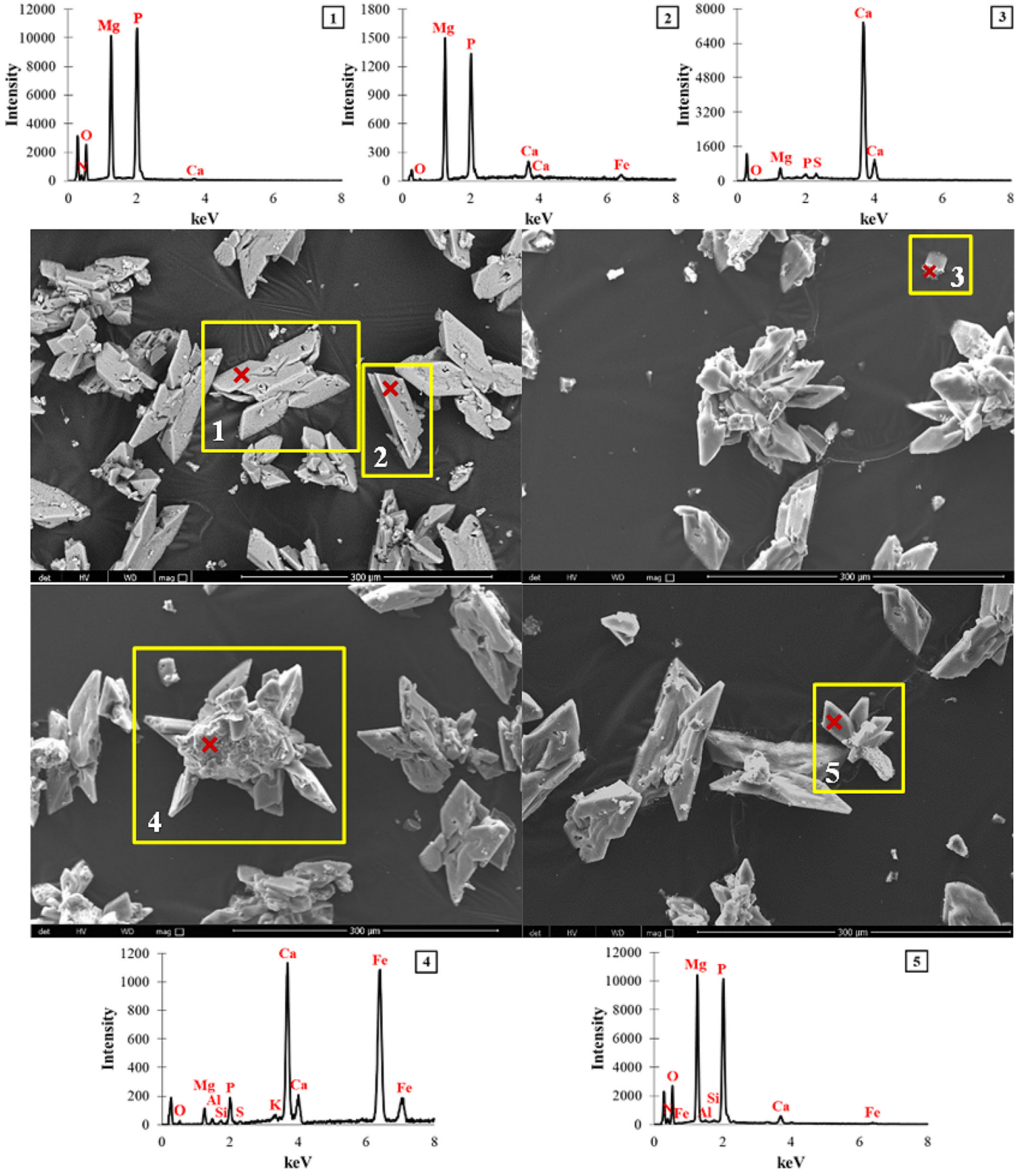

Fig. 6. Scanning electron micrograph of the precipitate and spots (red crosses) analysed by EDS to obtain information about the precipitate elemental composition. (1) hopper, (2) polyhedral, (3) partly-dissolved LG-MgO particle, (4) agglomeration of polyhedral on LG-MgO particles, and (5) agglomeration of polyhedral.

Catalunya for her predoctoral FI grant (2022 FI_B 00032). Sergi Astals is thankful to the Spanish Ministry of Science, Innovation and Universities for his Ramon y Cajal fellowship (RYC-2017-22372). Finally, the authors would like to thank the Catalan Government for the quality accreditation given to both research groups of the University of Barcelona (2021 SGR 00234, 2021 SGR 00708). DIOPMA (2021 SGR 00708) is a certified agent TECNIO in the category of technology developers from the Government of Catalonia.

References

Akyol, Ç., Foglia, A., Ozbayram, E.G., Frison, N., Katsou, E., Eusebi, A.L., Fatone, F., 2020. Validated innovative approaches for energy-efficient resource recovery and re-use from municipal wastewater: from anaerobic treatment systems to a biorefinery concept. Crit. Rev. Environ. Sci. Technol. 50, 869–902. https://doi.org/10.1080/10643389.2019.1634456.

Amann, A., Zoboli, O., Krampe, J., Rechberger, H., Zessner, M., Egle, L., 2018. Environmental impacts of phosphorus recovery from municipal wastewater. Resour. Conserv. Recycl. 130, 127–139. https://doi.org/10.1016/j.resconrec.2017.11.002.

Amaral, L.F., Salomão, R., Frollini, E., Pandolfelli, V.C., 2007. Mecanismos de hidratação do óxido de magnésio. Cerâmica 53, 368–372. https://doi.org/10.1590/S0366-69132007000400006.

Ariyanto, E., 2014. The influence of various physico-chemical process parameters on kinetics and growth mechanism of struvite crystallisation. Adv. Powder Technol. 13.

de-Bashan, L.E., Bashan, Y., 2004. Recent advances in removing phosphorus from wastewater and its future use as fertilizer (1997–2003). Water Res. 38, 4222–4246. https://doi.org/10.1016/j.watres.2004.07.014.

Battistoni, P., De Angelis, A., Pavan, P., Prisciandaro, M., Cecchi, F., 2001. Phosphorus removal from a real anaerobic supernatant by struvite crystallization. Water Res. 35, 2167–2178. https://doi.org/10.1016/S0043-1354(00)00498-X.

Bayuseno, A.P., Schmahl, W.W., 2020. Crystallization of struvite in a hydrothermal solution with and without calcium and carbonate ions. Chemosphere 250, 126245. https://doi.org/10.1016/j.chemosphere.2020.126245.

Bouzas, A., Martí, N., Grau, S., Barat, R., Mangin, D., Pastor, L., 2019. Implementation of a global P-recovery system in urban wastewater treatment plants. J. Clean. Prod. 227, 130–140. https://doi.org/10.1016/j.jclepro.2019.04.126.

Bradford-Hartke, Z., Lane, J., Lant, P., Leslie, G., 2015. Environmental benefits and burdens of phosphorus recovery from municipal wastewater. Environ. Sci. Technol. 49, 8611–8622. https://doi.org/10.1021/es505102v.

Bradford-Hartke, Z., Razmjou, A., Gregory, L., 2021. Factors affecting phosphorus recovery as struvite: effects of alternative magnesium sources. Desalination 504, 114949. https://doi.org/10.1016/j.desal.2021.114949.

Chimenos, J.M., Fernández, A.I., Villalba, G., Segarra, M., Urruticoechea, A., Artaza, B., Espiell, F., 2003. Removal of ammonium and phosphates from wastewater resulting from the process of cochineal extraction using MgO-containing by-product. Water Res. 37, 1601–1607. https://doi.org/10.1016/S0043-1354(02)00526-2.

Crutchik, D., Morales, N., Vázquez-Padín, J.R., Garrido, J.M., 2017. Enhancement of struvite pellets crystallization in a full-scale plant using an industrial grade magnesium product. Water Sci. Technol. 75, 609–618. https://doi.org/10.2166/wst.2016.527.

Desmidt, E., Ghyselbrecht, K., Monballiu, A., Rabaey, K., Verstraete, W., Meesschaert, B.D., 2013. Factors influencing urease driven struvite precipitation. Sep. Purif. Technol. 110, 150–157. https://doi.org/10.1016/j.seppur.2013.03.010.

van Dijk, K.C., Lesschen, J.P., Oenema, O., 2016. Phosphorus flows and balances of the European Union member states. Sci. Total Environ. 542, 1078–1093. https://doi.org/10.1016/j.scitotenv.2015.08.048.

Doyle, J.D., Parsons, S.A., 2002. Struvite formation, control and recovery. Water Res. 36, 3925–3940. https://doi.org/10.1016/S0043-1354(02)00126-4.

El Diwani, G., El Rafie, Sh., El Ibiari, N.N., El-Aila, H.I., 2007. Recovery of ammonia nitrogen from industrial wastewater treatment as struvite slow releasing fertilizer. Desalination 214, 200–214. https://doi.org/10.1016/j.desal.2006.08.019.

Elduayen-Echave, B., Azcona, M., Grau, P., Schneider, P.A., 2020. Effect of the shear rate and supersaturation on the nucleation and growth of struvite in batch stirred tank reactors. J. Water Process. Eng. 38, 101657.

Fromberg, M., Pawlik, M., Mavinic, D.S., 2020. Induction time and zeta potential study of nucleating and growing struvite crystals for phosphorus recovery improvements within fluidized bed reactors. Powder Technol. 360, 715–730. https://doi.org/10.1016/j.powtec.2019.09.067.

Hao, X.-D., Wang, C.-C., Lan, L., van Loosdrecht, M.C.M., 2008. Struvite formation, analytical methods and effects of pH and Ca2 +. Water Sci. Technol. 58, 1687–1692. https://doi.org/10.2166/wst.2008.557.

Kataki, S., West, H., Clarke, M., Baruah, D.C., 2016. Phosphorus recovery as struvite from farm, municipal and industrial waste: feedstock suitability, methods and pretreatments. Waste Manag. 49, 437–454. https://doi.org/10.1016/j.wasman.2016.01.003.

Kazadi Mbamba, C., Tait, S., Flores-Alsina, X., Batstone, D.J., 2015. A systematic study of multiple minerals precipitation modelling in wastewater treatment. Water Res. 85, 359–370. https://doi.org/10.1016/j.watres.2015.08.041.

Kok, D.-J.D., Pande, S., van Lier, J.B., Ortigara, A.R.C., Savenije, H., Uhlenbrook, S., 2018. Global phosphorus recovery from wastewater for agricultural reuse. Hydrol. Earth Syst. Sci. 22, 5781–5799. https://doi.org/10.5194/hess-22-5781-2018.

Liu, X., Wang, J., 2019. Impact of calcium on struvite crystallization in the wastewater and its competition with magnesium. Chem. Eng. J. 378, 122121. https://doi.org/10.1016/j.cej.2019.122121.

Marti, N., Bouzas, A., Seco, A., Ferrer, J., 2008. Struvite precipitation assessment in anaerobic digestion processes. Chem. Eng. J. 141, 67–74. https://doi.org/10.1016/j.cej.2007.10.023.

Martí, N., Pastor, L., Bouzas, A., Ferrer, J., Seco, A., 2010. Phosphorus recovery by struvite crystallization in WWTPs: influence of the sludge treatment line operation. Water Res. 44, 2371–2379. https://doi.org/10.1016/j.watres.2009.12.043.

Muys, M., Phukan, R., Brader, G., Samad, A., Moretti, M., Haiden, B., Pluchon, S., Roest, K., Vlaeminck, S.E., Spiller, M., 2021. A systematic comparison of commercially produced struvite: quantities, qualities and soil-maize phosphorus availability. Sci. Total Environ. 756, 143726. https://doi.org/10.1016/j.scitotenv.2020.143726.

Park, N., Chang, H., Jang, Y., Lim, H., Jung, J., Kim, W., 2021. Prediction of adequate pH and mg 2 + dosage using an empirical MgO solubility model for struvite crystallization. Environ. Technol. Innov. 21, 101347. https://doi.org/10.1016/j.eti.2020.101347.

Pastor, L., Mangin, D., Barat, R., Seco, A., 2008. A pilot-scale study of struvite precipitation in a stirred tank reactor: conditions influencing the process. Bioresour. Technol. 99, 6285–6291. https://doi.org/10.1016/j.biortech.2007.12.003.

Quintana, M., Colmenarejo, M.Fco, Barrera, J., García, G., García, E., Bustos, A., 2004. Use of a byproduct of magnesium oxide production to precipitate phosphorus and nitrogen as struvite from wastewater treatment liquors. J. Agric. Food Chem. 52, 294–299. https://doi.org/10.1021/jf0303870.

Quintana, M., Sánchez, E., Colmenarejo, M.F., Barrera, J., García, G., Borja, R., 2005. Kinetics of phosphorus removal and struvite formation by the utilization of by-product of magnesium oxide production. Chem. Eng. J. 111, 45–52. https://doi.org/10.1016/j.cej.2005.05.005.

Quintana, M., Colmenarejo, M.F., Barrera, J., Sánchez, E., García, G., Travieso, L., Borja, R., 2008. Removal of phosphorus through struvite precipitation using a by-product of magnesium oxide production (BMP): Effect of the mode of BMP preparation. Chem. Eng. J. 136, 204–209. https://doi.org/10.1016/j.cej.2007.04.002.

Rahman, Md.M., Salleh, M.A.Mohd, Rashid, U., Ahsan, A., Hossain, M.M., Ra, C.S., 2014. Production of slow release crystal fertilizer from wastewaters through struvite crystallization – a review. Arab. J. Chem. 7, 139–155. https://doi.org/10.1016/j.arabjc.2013.10.007.

Romero-Güiza, M.S., Tait, S., Astals, S., del Valle-Zermeño, R., Martínez, M., Mata-Alvarez, J., Chimenos, J.M., 2015. Reagent use efficiency with removal of nitrogen from pig slurry via struvite: a study on magnesium oxide and related by-products. Water Res. 84, 286–294. https://doi.org/10.1016/j.watres.2015.07.043.

Santos, A.F., Almeida, P.V., Alvarenga, P., Gando-Ferreira, L.M., Quina, M.J., 2021. From wastewater to fertilizer products: alternative paths to mitigate phosphorus demand in European countries. Chemosphere 284, 131258. https://doi.org/10.1016/j.chemosphere.2021.131258.

Sena, M., Seib, M., Noguera, D.R., Hicks, A., 2021. Environmental impacts of phosphorus recovery through struvite precipitation in wastewater treatment. J. Clean. Prod. 280, 124222. https://doi.org/10.1016/j.jclepro.2020.124222.

Shaddel, S., 2019. Engineering of struvite crystals by regulating supersaturation – correlation with phosphorus recovery, crystal morphology and process efficiency. Journal of environmental. Chem. Eng. 9.

Siciliano, A., Limonti, C., Curcio, G.M., 2020. Advances in Struvite Precipitation Technologies for Nutrients Removal and Recovery from Aqueous Waste and Wastewater. p. 36.

Stolzenburg, P., Capdevielle, A., Teychené, S., Biscans, B., 2015. Struvite precipitation with MgO as a precursor: application to wastewater treatment. Chem. Eng. Sci. 133, 9–15. https://doi.org/10.1016/j.ces.2015.03.008.

Strydom, C.A., 2005. The Effect of Calcining Conditions on the Rehydration of Dead Burnt Magnesium Oxide Using Magnesium Acetate as a Hydrating Agent 4.

Uysal, A., Yilmazel, Y.D., Demirer, G.N., 2010. The determination of fertilizer quality of the formed struvite from effluent of a sewage sludge anaerobic digester. J. Hazard. Mater. 181, 248–254. https://doi.org/10.1016/j.jhazmat.2010.05.004.

del Valle-Zermeño, R., Giro-Paloma, J., Formosa, J., Chimenos, J.M., 2015. Low-grade magnesium oxide by-products for environmental solutions: characterization and geochemical performance. J. Geochem. Explor. 11.

del Valle-Zermeño, R., Formosa, J., Gómez-Manrique, J., Chimenos, J.M., 2016. Desulfurization performance of MgO byproducts as a function of particle size. Energy Fuel 30, 2328–2335. https://doi.org/10.1021/acs.energyfuels.6b00041.

Vinardell, S., 2021. Co-digestion of sewage sludge and food waste in a wastewater treatment plant based on mainstream anaerobic membrane bioreactor technology: a techno-economic evaluation. Bioresour. Technol. 11.

Ye, Y., Ngo, H.H., Guo, W., Liu, Yiwen, Li, J., Liu, Yi, Zhang, X., Jia, H., 2017. Insight into chemical phosphate recovery from municipal wastewater. Sci. Total Environ. 576, 159–171. https://doi.org/10.1016/j.scitotenv.2016.10.078.